Thermodynamics of hydronium and hydroxide surface solvation - Supporting information

Jochen S. Hub[1,†]   Maarten G. Wolf[2,†]   Carl Caleman[3,4]
Paul J. van Maaren[5]   Gerrit Groenhof[2,6]
David van der Spoel[5,*]

December 3, 2013

[1] Institute for Microbiology and Genetics, Georg-August-University Göttingen, Justus-von-Liebig-Weg 11, D-37077 Göttingen, Germany

[2] Computational Biomolecular Chemistry, Max Planck Institute for Biophysical Chemistry, Am Fassberg 11, D-37077 Göttingen, Germany

[3] Center for Free-Electron Laser Science, DESY, Notkestraße 85, D-22607 Hamburg, Germany

[4] Department of Physics and Astronomy, Uppsala University, Box 516, SE-75120 Uppsala, Sweden

[5] Uppsala Center for Computational Chemistry, Science for Life Laboratory, Department of Cell and Molecular Biology, Uppsala University, Husargatan 3, Box 596, SE-75124 Uppsala, Sweden

[6] Department of Chemistry and Nanoscience center, University of Jyväskylä, P.O. Box 35 FI-40014 Jyväskylä, Finland

[†] Contributed equally to this work

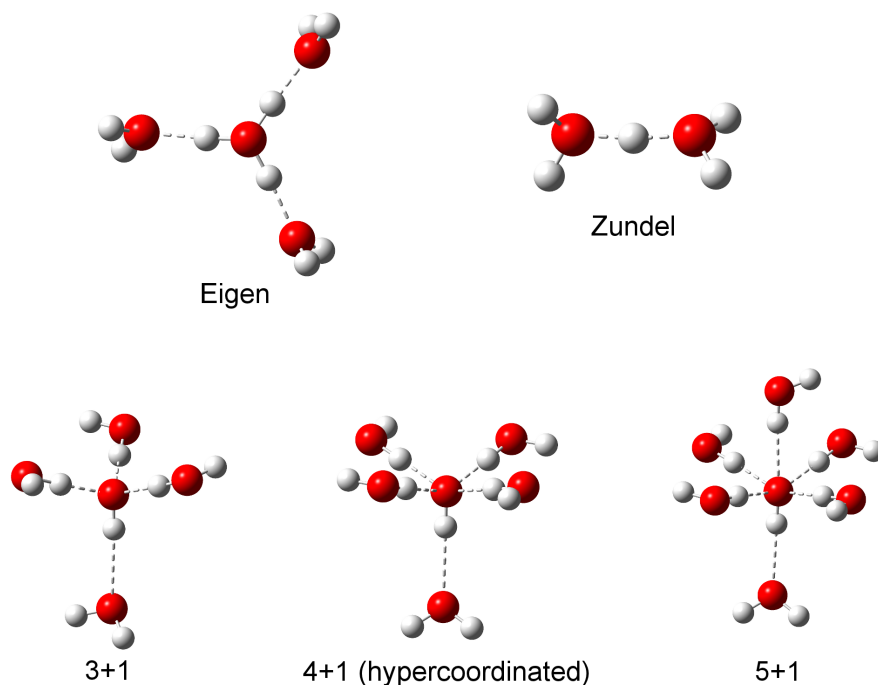* corresponding author email: david.vanderspoel@icm.uu.se

Figure S1: Hydronium and hydroxide complexes in water. X and Y in X+Y refer to the number of hydrogen bonds with O* and H*, respectively. Other observed hydroxide species are 3+0, 4+0 and 5+0.

1 Methods

1.1 Model development

Quantum calculations were performed with the gaussian03 package [1] at both the mp2 [2, 3]/6-311+g** [4–7] and the b3lyp [8–10]/aug-cc-pvtz [11–13] levels of theory unless stated otherwise. The structures of isolated hydronium and hydroxide ions were optimized using the PCM implicit solvent [14, 15] to extract the internal structure parameters. We applied the procedure described by Anisimov *et al.* [16] to obtain atomic and drude partial charges.

Reference energy profiles of water dissociation from the hydronium or hydroxide were calculated by changing the distance between the water oxygen (Ow) and the hydronium or hydroxide oxygen (O*). Starting from the optimized complex the position of the water oxygen was varied along the O*-Ow vector. To maintain the symmetry of the ion-water complexes, equivalent wa-

ters were dissociated simultaneously. For every O*-Ow distance the structure was optimized at the b3lyp/aug-cc-pvtz or MP2/6-311+g** level, with the oxygen positions frozen. The energies were then calculated at the b3lyp/aug-cc-pvtz or CCSD [17]/6-311+g** level including counterpoise correction to the basis-set superposition error [18].

The force field energy profiles were calculated based on the b3lyp optimized structures, applying infinite van der Waals and coulomb cut-off and no periodic boundary conditions. Before the energy was calculated the bond distances in the hydronium or hydroxide and water were constrained, using the SHAKE [19] and SETTLE [20] algorithms, respectively.

The new models are available from the GROMACS Molecule and Liquid database [21] at `http://virtualchemistry.org`.

1.2 Molecular dynamics simulations

Bulk water simulations   The molecular dynamics (MD) simulations were first done in bulk water to verify the new models. Those simulations were done in a cubic box containing the ion and 712 SWM4-NDP water molecules[22]. Bond distance were constrained similar to the energy calculations and a time step of 2 fs was used. The temperature was connected to a heat bath of 300 K using velocity rescaling[23] with τ_t set to 0.5 ps. For the bulk water simulations, the pressure was maintained constant at 1 atm using the Berendsen barostat [24] with τ_p set to 1.0 ps and a compressibility of $4.5 \cdot 10^{-5}$ bar^{-1}. Van der Waals interactions were cut-off at 1.2 nm and the electrostatic interactions were treated using the particle-mesh Ewald method [25] with a real space cut-off of 0.9 nm. Since we did not neutralize the system with a counter ion, the system was implicitly neutralized by the Ewald method by means of a neutralizing background charge (or neutralizing plasma). Neighbour searching was performed every 5 steps with a 0.9 nm cut-off for the short-range neighbour list. Simulations of the parameter derivation and model validation sampled 0.1 and 10 ns, respectively.

Slab geometry   For the slab geometry no pressure coupling was used, and the z box-vector was increased to 20 nm, creating a water slab spanning the xy plane. For hydroxide simulations we increased the number of water molecules to 2692. We simulated 100 copies of the slab geometry in parallel, sampling a total of 4 and 1 μs for the hydronium and hydroxide, respectively. Free energy profiles were calculated over 100 ns trajectories, based on the

4

distribution of the oxygen atom over the slab. The mean and standard error are then calculated for the obtained set of free energy profiles.

1.3 Potential of mean force calculations in the droplet

Potentials of mean force for the water droplet were computed as detailed elsewhere [26], using a droplet of 215 SWM4-NDP water molecules[22]. In short, hydronium, hydroxide, or a water molecule was constrained at different distances r from the center of mass of a water droplet, with $0.05\,\mathrm{nm}$ between adjacent positions. The polarizable water model SWM4-NDP due to Lamoureux and Roux was used[27] in conjunction with the hydronium and hydroxide models developed in this work. Since droplets in the gas phase were studied, no cut-offs for Lennard-Jones or Coulomb interactions were needed, and no periodic boundary conditions were applied. Hence, because no Ewald summation was used for the electrostatics in those simulations, there was no requirement to neutralize the simulation system by means of counter ions. The temperature was controlled using a stochastic dynamics integrator [28] with a time constant of 0.1 ps. An integration time step of 2 fs was employed and sampling was performed for 20 ns at each r. The mean forces on the ions were computed disregarding the first 50 ps of each trajectory for equilibration, and the PMF was computed by integration of the mean force. Statistical errors were computed by binning analysis [29]. The GROMACS software [30, 31] was used for all simulations.

$\Delta H(r)$ was computed from the average potential energy of the system relative to the central region. Because the volume was constant (infinite) and the temperature was controlled the constant contribution from the temperature was considered not to affect the relative enthalpies. The entropic contribution to the PMFs was henceforth computed as

$$-T\Delta S(r) = \Delta G(r) - \Delta H(r), \tag{1}$$

where $G(r)$ denotes the PMF. The interaction energies $\langle\Delta V_{\text{solute-water}}(r)\rangle$ and $\langle\Delta V_{\text{water-water}}(r)\rangle$ were computed by averaging of the sum of the respective Lennard-Jones and Coulomb interactions. Here, the polarization energy of solute and water were attributed to solute-water and water-water interactions, respectively.

1.4 Surface tension calculations

The effect of NaOH on the surface tension γ was computed using 148 ns simulations of pure water (1696 molecules) and NaOH solutions at four different concentrations (S3). The model for sodium was taken from Yu *et al.* [32]. Simulation parameters were the same as above, except that an elongated box of 4x4x12 nm was used under constant volume conditions and that lattice sums were used for evaluating the Lennard-Jones interactions [33], since, as some authors have pointed out that surface tension is especially sensitive to cut-off treatment [34, 35]. We note, however, that the slope of γ as well as the reduced OH^- concentration at the surface were nearly identical if Lennard-Jones cutoffs were used instead (not shown). Errors were computed by binning analysis [29].

2 Results

2.1 Hydronium and hydroxide parameter derivation

The hydronium and hydroxide models were parameterized based on ab initio data. The bond length and angles were extracted from an implicit solvent optimized H_3O^+ or OH^- structure, and the partial charges were derived analogous to previously described ion parametrization [16].

The van der Waals parameters were optimized to best represent energy profiles of water-ion dissociation. In our models, the strong attraction between the hydronium or hydroxide and water is purely coulombic, and the van der Waals attraction is negligible small. The repulsion term, however, is necessary to prevent atomic overlap. Since the Lennard-Jones potential has two free parameters, and we fitted to just one parameter, we had some freedom in choosing ϵ and σ. To ensure that the interaction strength towards non-charged species is reasonable, we set ϵ to obtain a van der Waals well depth equal to the water model. With ϵ fixed σ was optimized to match the water dissociation energy profile, with an emphasis on the position of the minimum.

	Hydronium	Hydroxide
q_O (e)	0.852	0.202
q_{OS} (e)	-1.124	-1.432
q_H (e)	0.424	0.23[1]
ϵ (kcal/mol)	0.2109	0.0703
σ_O (Å)	3.15	-
σ_{V1} (Å)	-	2.8
σ_{V2} (Å)	-	2.4
σ_{HH} (Å)	-	0.7

[1]Positioned on q_H in S2

Table S1: Non-bonded parameters for hydronium and hydroxide.
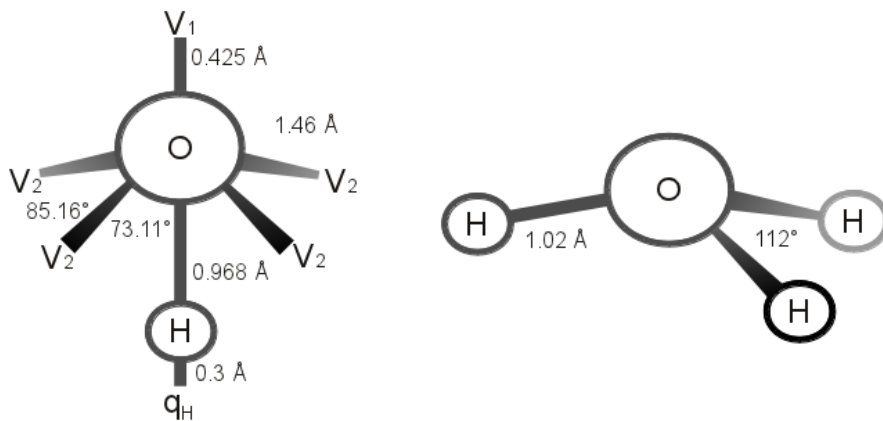

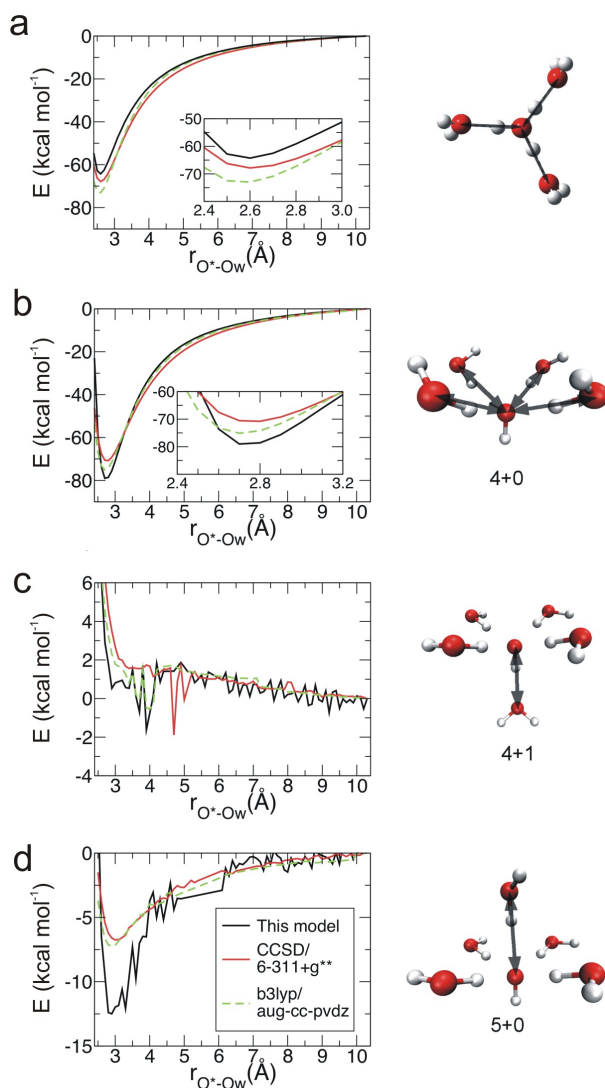**Figure S2:** Structure of our hydroxide (left) and hydronium (right) model.

Figure S3: Energy profile associated to water dissociation from a hydronium (a) or a hydroxide (b-d). The arrows indicate the direction and number of dissociated water molecules. The energy profiles are shifted such that the energy is zero at a hydronium-oxygen–water-oxygen (O*-Ow) distance of 10.4Å. The dips in the (4+1) energy profiles (c) are caused by different orientations of the water hydrogen bonded to H*. During optimization with implicit solvent two water orientations had almost equal energy, but in vacuum these energies were no longer equal. Note that the MM energy profile based on the b3lyp/aug-cc- pvtz structures show exactly the same energy dips as the b3lyp/aug-cc-pvtz energy profile.

8

The resulting hydronium model, S2 and S1, has bond length and angle in accord with the $H_3O^+ \cdot 3H_2O$ QM structures of this work and others[36, 37]. Also, within the limits of force field approaches, the agreement between the final MM and the QM water dissociation energy profiles is very good (S3).

For the hydroxide we required a more complex model to prevent overcoordination, due to an anomalous increase of the water concentration in the volume around the O*-H* bond (see for example Figure 1 a and b in ref [38]). To exclude water molecules from this volume, we described the van der Waals interaction by six Lennard-Jones potentials instead of one. Four were placed symmetrically around the O*-H* bond, one centered at the hydrogen and one at the opposite side of O*, in S2 denoted by V_2, H and V_1, respectively.

Ideally, we would like to define the V_1 and V_2 sites as virtual sites. For V_1 that is no problem, but the position of V_2 cannot be defined based only on the O* and H* position. Therefore, we treated each V_2 site as a particle with mass 1 a.u. and subtracted the total of 4 a.u. from the oxygen mass. We constrained the O-V_2 and closest V_2-V_2 distances and added a harmonic potential for the H-O-V_2 and V_2-V_2-V_2 angles with a force constant of 163 and 96 kcal mol^{-1}, respectively.

The optimal position of V_1 and V_2 were obtained via a grid search of various distances to O*. For every unique combination of V_1 and V_2 positions the Lennard-Jones parameters were rederived. In this model at most three hydroxide Lennard-Jones minima overlap at any one point in space, and, therefore, we set the hydroxide ϵ to one third of the water ϵ. With ϵ fixed, σ_{V_1} was fitted to the energy profile of one water dissociating from the $OH^- \cdot [5 + 0H_2O]$ cluster and σ_{V_2} to the simultaneous dissociation of four water molecules from the $OH^- \cdot [4 + 0H_2O]$ cluster (S3).

We were unable to match the (5+0) energy profile with our MM model, because there is a large charge delocalization in the QM structure [38–40] that could not be mimicked in our MM model. Since the 5-fold coordination state is only marginally populated, the energetic effect of the hydroxide in solution will be small. The MM energy profiles of 4-fold coordinated complex, the dominant state in solution, agree well to the QM profiles.

At this point, merely appropriate hydrogen bond acception was missing in our hydroxide model. We found that the associated MM interaction energy was too high compared to the QM result, reducing the hydrogen bond capability. A significant contribution to this energy is the O*-Ow coulomb interaction. In the QM simulation the negative charge is delocalized over the hypercoordinated water molecules [38–40] thereby reducing the O*-Ow

9

coulomb repulsion. As we could not reduce the total charge of the hydrox-
ide, we placed the hydrogen charge (q_H) further out, to increase the H*-Ow
coulomb attraction and balance the too high O*-Ow coulomb repulsion (S2).
We fitted the H* Lennard-Jones parameters for each q_H position to the en-
ergy profile of one water dissociating from the $OH^- \cdot [4 + 1H_2O]$ (S3). By
bringing the proton charge out to 0.3 Å from the H* center, q_H in S2, we
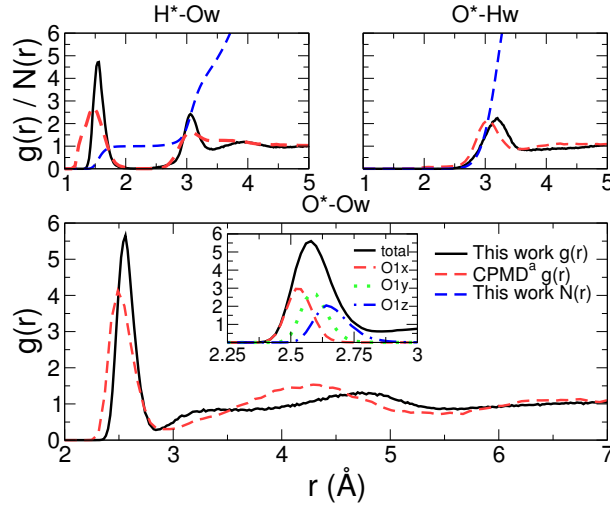obtained the appropriate hydrogen bonding properties.

2.2 Model validation

Figure S4: Hydronium-water radial distribution functions. For H*-Ow and O*-
Hw also the cumulative radial distribution N(r) is given. Inset in the O*-Ow graph
is the distance distributions between O* and the first, second and third closest Ow
(O1x, O1y and O1z, respectively). The CPMD data are obtained from Knight *et
al.* [41].

Simulating a hydronium in solution using our new model resulted in an
average distance between the hydronium and water oxygen (O* and Ow) of
2.55 Å(S4). This is in good agreement with the results of ab initio simulations
(2.53-2.60 Å) [36, 41–45] and x-ray crystallography (2.55-2.57) [46, 47] that
are dominated by Eigen complexes. On the other hand, neutron diffraction
experiments of very concentrated HCl solutions [48] and other ab initio cal-
culations [37, 49] that display more Zundel character [37, 49, 50] show smaller

O*-Ow distances (2.48 and 2.4-2.5 Å, respectively). We do observe a shift in the position of the second O*-Ow maximum with respect to the CPMD results (S4). This is also present in other hydronium models [41] and probably originates in the fixed bond length in the force fields.

As expected for an Eigen complex, the hydronium donated three hydrogen bonds, one from each hydrogen H*-Ow (S4). In addition, we observed no significant hydrogen bond accepting capability in our models O*-Hw (S4). These features are in good agreement with ab initio calculations [37, 42] and neutron diffraction experiments [48].

In solution the Eigen complex forms a dynamically distorted asymmetric complex. The O*-Ow distances are not equidistant and the water participating in the shortest hydrogen bond is continuously changing [42–44, 51]. We reproduced this distorted asymmetric structure with different hydrogen bond lengths between the hydronium and the first three waters very well (inset in S4). We observed an average exchange time of the identity of the first and second closest water of 26 fs, comparable to *ab initio* calculations [43]. The average identity exchange between second and third closest water is slightly faster with 15 fs.
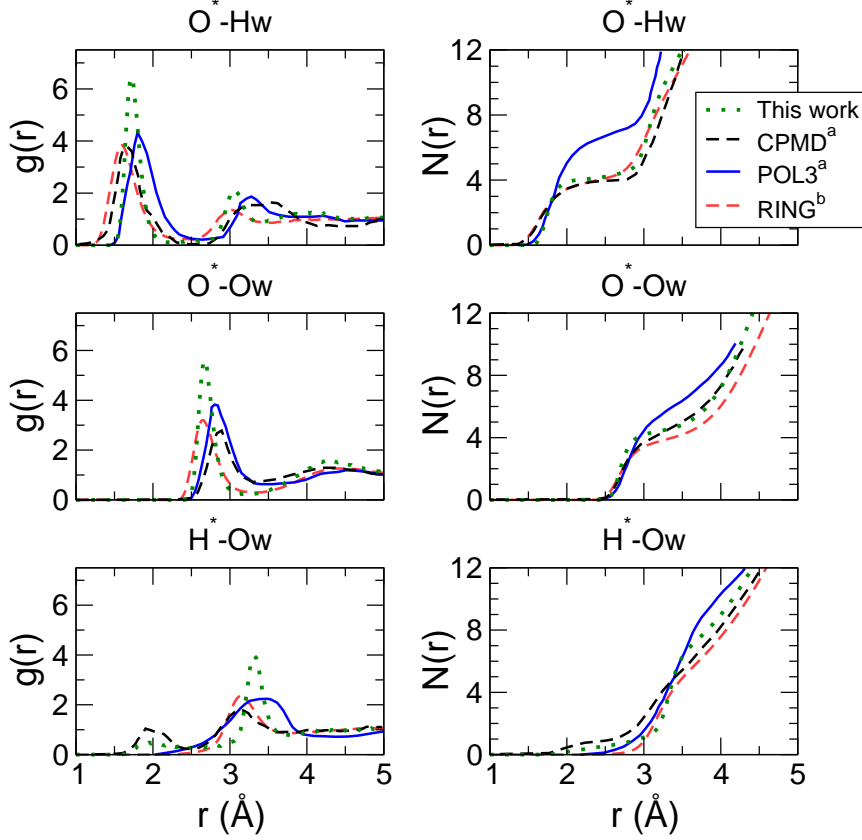
Figure S5: Hydroxide-water radial distribution functions. The standard g(r) and cumulative N(r) radial distribution functions of water oxygen Ow and hydrogen Hw around the hydroxide oxygen O* and hydrogen H*. The CPMD and POL3 data are obtained from Bucher *et al.* [38], and the RING model data from Ufimtsev *et al.* [52].

Simulating a hydroxide in water with our new model lead to a coordination number of 4.4 at the first O*-Ow minimum (S5). This value is close to the coordination number of 4.2 obtained by neutron scattering of a diluted NaOH solution (2M) [53]; 4.3 to 4.8 from x-ray / ab initio at concentrated (15.5 M) to medium/diluted (smaller than 8.8 M) solution, respectively [54], and of ~4.5 from ab initio calculations [38–40, 52]. Furthermore, we found a peak distance of the O*-Ow radial distribution function of 2.7 Å(S5). This is in good agreement with 2.65 - 2.77 Å observed in FTIR and X-ray scattering experiments and *ab-initio* calculations [38, 54, 55]. Only the O*-Ow

distance from a neutron-scattering/ Monte Carlo sampling experiment of 2.3 Å [53, 56] disagree. However, the hydroxide model used during the Monte Carlo sampling was a simple point charge model. With a reasonable size of the hydroxide van der Waals sphere such models result in overcoordinated complexes [38, 52]. We speculate that the best fit to the scattering data arose with the correct coordination number, which could be reached all the same by decreasing the size of the hydroxide van der Waals sphere. As a result, the O*-Ow distance was significantly decreased.

Furthermore, we observed four accepted hydrogen bonds by the hydroxide with an average O*-Hw distance of 1.7 Å (S5 O*-Hw). This lead to a plateau in the O*-Hw cumulative radial distribution function at N(r)=4, that is characteristic for the hypercoordinated structure [38, 52]. In addition, we found a weak hydrogen bond, donated by the hydroxide, with an average H*-Ow distance of 2.0 Å (S5). The coordination number associated to this interaction was 0.53, in good agreement with the experimental observed weak hydrogen bonding [53, 55, 56] as well as with ab initio simulations [38–40, 52].

The only other hydroxide model that yielded an average coordination number of 4 was the ring model developed by Ufimtsev et $al.$ [52]. However, the cumulative O*-Ow as well as the weak hydrogen bond donation produced by the ring model do not agree well with the CPMD data (S5). An additional drawback of the ring model is the strong exponential repulsive term that is introduced (equation 4 in [52]). This term is parameterized for the hydroxide in water, but the effect of this term in another environment or at a surface is unclear. Finally, the lack of polarizability makes this model unsuitable to investigate water surface properties.

2.3   Slab PMF

In order to further validate the PMFs from solvation in a droplet, the potential of mean force in a slab geometry was computed as well (S6). The overall appearance is very similar to that in a droplet, with an energy minimum for hydronium at -2.5 kJ/mol (-3 kJ/mol in the droplet geometry) and an energy maximum of +3 kJ/mol for hydroxide (+4 kJ/mol in the droplet).
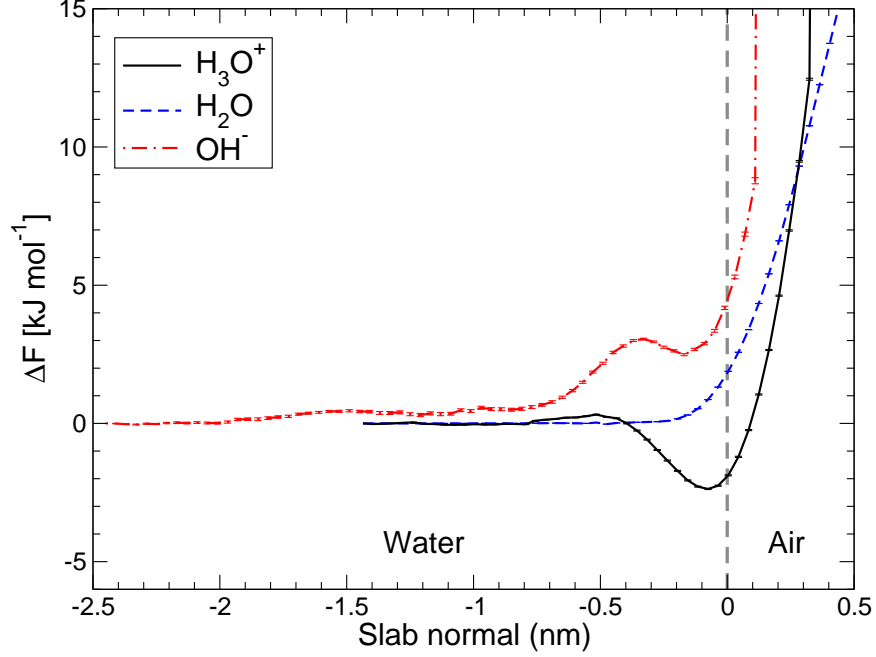
Figure S6: Free energy profile in a slab geometry, that is with periodicity in two dimensions, for hydronium, water and hydroxide.

2.4 Computation of the p[H], p[OH] and pK$_\mathrm{w}$

In contrast to the pH that is defined through the activity of H_3O^+, the p[H] on the droplet surface reflects the concentration of H_3O^+ in the top layer. Based on Fig. 3 in the main text we consider the surface layer for H_3O^+ as the layer between $r_i = 0.75$ nm and the Gibbs dividing surface at $r_o = 1.1$ nm. The surface concentration c_s in this layer is determined by

$$c_s = c_i \cdot f = c_i \cdot \frac{\int_{r_i}^{r_o} 4\pi r^2 \exp[-\Delta G(r)/k_B T] \mathrm{d}r}{\int_{r_i}^{r_o} 4\pi r^2 \mathrm{d}r}, \tag{2}$$

where c_i is the hydronium concentration in the bulk, and f a factor computed from the PMF. Thus, we here compute p[H] from the *average* hydronium concentration in the outermost slab, rather than from the minimum of the hydronium PMF, as for instance done by Buch *et al.* [57]. The difference in

Table S2: Effect of the affinities of hydronium and hydroxide on the surface acidity and dissociation constant.

Molecule	Droplet	Slab
Δp[H]	-0.3	-0.3
Δp[OH]	0.9	0.5
ΔpK$_\mathrm{w}$	0.6	0.2

p[H] at the surface and the bulk is

$$\Delta\mathrm{p[H]} = -(\log_{10}(c_s) - \log_{10}(c_i)) = -\log_{10} f. \tag{3}$$

Using the PMF for hydronium (Fig. 3A), one arrives at $\Delta\mathrm{p[H]} \approx -0.3$, corresponding to a slightly enhanced hydronium concentration at the surface as compared to the bulk (S2). Following the same calculation yields the difference in p[OH] compared to the bulk to $\Delta\mathrm{p[OH]} \approx +0.9$, corresponding to a reduced OH$^-$ concentration at the surface. Note that, because the PMFs of hydronium and hydroxide, $\mathrm{PMF}_{\mathrm{H_3O^+}}(r) + \mathrm{PMF}_{\mathrm{OH^-}}(r)$, do not sum up to zero, the autodissociation constant of water pK$_\mathrm{w}$ is different at the surface compared to the bulk.

In the slab simulations 2 simplifies to

$$c_s = c_i \cdot f = c_i \cdot \frac{\int_{r_i}^{r_o} \exp[-\Delta G(r)/k_B T]\mathrm{d}r}{\int_{r_i}^{r_o} \mathrm{d}r}, \tag{4}$$

and the corresponding numbers are given in S2. For the (infinite) slab case we find the same change in p[H] as we do for the droplet (-0.3 p[H] units).

2.5 Computation of orientational entropy

The Shannon entropy of the orientational distribution of hydroxide was computed as

$$S(r) = -R \int_{-1}^{1} P_n(r, \cos(\theta)) \ln[P_n(r, \cos(\theta))] \, \mathrm{d}\cos(\theta), \tag{5}$$

where R is the gas constant. $P_n(r, \cos(\theta))$ denotes the orientational probability normalized for each position r, that is,

$$P_n(r, \cos(\theta)) = P(r, \cos(\theta)) / \int_{-1}^{1} P(r, \cos(\theta)) \, \mathrm{d}\cos(\theta) \tag{6}$$

15

Table S3: Surface tension γ (mN/m) in water with different salt concentrations. The statistical error was determined a binning analysis over a total of 218 ns of simulation for each concentration.[29].

#Water	#NaOH	[NaOH]	γ
1696	0	0	61.7 ± 0.16
1696	16	0.5 M	62.2 ± 1.6
1696	32	1.0 M	62.6 ± 0.17
1696	48	1.5 M	63.0 ± 0.17
1696	64	2.0 M	63.0 ± 0.18

2.6 Surface tension

The density profile generated by a 1M sodium hydroxide solution is plotted in S7C. Clearly, the ions are distributed predominantly below the Gibbs dividing surface. The corresponding surface tensions γ from five sets of simulations are listed in S3 and plotted in S7A. In qualitative agreement to experiments, we find that γ increases with [NaOH]. However, the SWM4-NDP predicts a too low γ, and the slope $\Delta\gamma/[\text{NaOH}]$ is $0.85\,\text{mNm}^{-1}\text{M}^{-1}$, which is smaller than the experimental value of $2.0\,\text{mNm}-1\text{M}-1$ (S7) [58]. These findings demonstrate, in short, that the surface tension increases despite the fact that the hydroxide and sodium ions are predominantly located in the bulk.
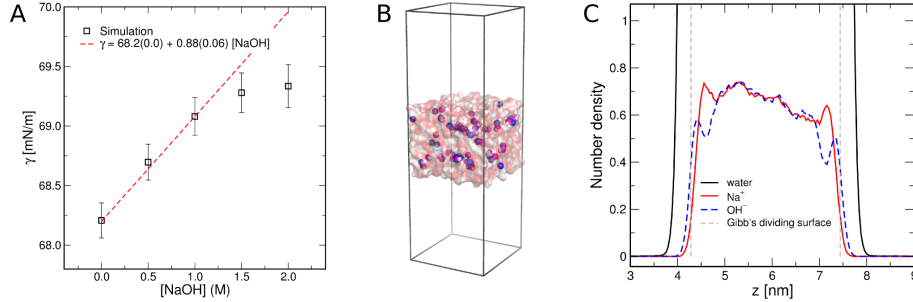

Figure S7: (A) Surface tension γ as a function of NaOH concentration in water. (B) Water slab simulation system used to compute γ, here showing 1M [NaOH] concentration. (C) Density profile of Na^+ (solid red) and OH^- (dashed blue) ions in a water slab during surface tension calculations (at 1M [NaOH]). Averaged over 218 ns of simulation. OH^- concentration is reduced at the surface as compared to the bulk. The Gibb's dividing surfaces are indicated as grey dashed lines

References

[1] Frisch, M. J., Trucks, G. W., Schlegel, H. B., and M. A. Robb, G. E. S., Cheeseman, J. R., Jr., J. A. M., and K. N. Kudin, T. V., Burant, J. C., Millam, J. M., Iyengar, S. S., and V. Barone, J. T., Mennucci, B., Cossi, M., Scalmani, G., and G. A. Petersson, N. R., Nakatsuji, H., Hada, M., Ehara, M., Toyota, K., Fukuda, R., Hasegawa, J., Ishida, M., Nakajima, T., Honda, Y., Kitao, O., Nakai, H., Klene, M., Li, X., Knox, J. E., Hratchian, H. P., Cross, J. B., Bakken, V., Adamo, C., Jaramillo, J., Gomperts, R., Stratmann, R. E., Yazyev, O., Austin, A. J., Cammi, R., Pomelli, C., Ochterski, J. W., Ayala, P. Y., Morokuma, K., Voth, G. A., Salvador, P., Dannenberg, J. J., Zakrzewski, V. G., Dapprich, S., Daniels, A. D., Strain, M. C., Farkas, O., Malick, D. K., Rabuck, A. D., Raghavachari, K., Foresman, J. B., Ortiz, J. V., Cui, Q., Baboul, A. G., Clifford, S., Cioslowski, J., Stefanov, B. B., Liu, G., Liashenko, A., Piskorz, P., Komaromi, I., Martin, R. L., Fox, D. J., Keith, T., Al-Laham, M. A., Peng, C. Y., Nanayakkara, A., Challacombe, M., Gill, P. M. W., Johnson, B., Chen, W., Wong, M. W., Gonzalez, C., and Pople, J. A. Gaussian 03, revision d.01. Gaussian, Inc., Wallingford CT, (2004).

[2] Moller, C. and Plesset, M. *Phys. Rev.* **46**, 619 (1934).

[3] Pople, J. A., Krishnan, R., Schlegel, H. B., and Binkley, J. S. *Int. J. Quantum Chem. Symp.* **13**, 325 (1979).

[4] McLean, A. D. and Chandler, G. S. *J. Chem. Phys.* **72**, 5639 (1980).

[5] Krishnan, R., Binkley, J. S., Seeger, R., and Pople, J. A. *J. Chem. Phys.* **72**, 650 (1980).

[6] Clark, T., Chandrasekhar, J., Spitznagel, G., and Schleyer, P. *J. Comput. Chem.* **4**, 294 (1983).

[7] Frisch, M. J., Pople, J. A., and Binkley, J. S. *J. Chem. Phys.* **80**, 3265 (1984).

[8] Becke, A. *J. Chem. Phys.* **98**, 5648 (1993).

[9] Becke, A. *Phys. Rev.* **38**, 3098 (1988).

[10] Lee, C., Yang, W., and Parr, R. G. *Phys. Rev. B* **37**, 785 (1988).

[11] Dunning Jr., T. H. *J. Chem. Phys.* **90**, 1007 (1989).

[12] Kendall, R. A., Dunning Jr., T. H., and Harrison, R. J. *J. Chem. Phys.* **96**, 6796 (1992).

[13] Wilson, A. K., van Mourik, T., and Dunning Jr., T. H. *J. Mol. Struct: THEOCHEM* **388**, 339 (1997).

[14] Tomasi, J., Mennucci, B., and Cammi, R. Quantum mechanical continuum solvation models. *Chem. Rev.* **105**, 2999–3093 (2005).

[15] Foresman, J. B., Keith, T. A., Wiberg, K. B., Snoonian, J., and Frisch, M. J. Solvent effects 5. the influence of cavity shape, truncation of electrostatics, and electron correlation on ab initio reaction field calculations. *J. Phys. Chem.* **100**, 16098–104 (1996).

[16] Anisimov, V. M., Lamoureux, G., Vorobyov, I. V., Huang, N., Roux, B., and MacKerell, Jr., A. D. Determination of electrostatic parameters for a polarizable force field based on the classical drude oscillator. *J. Chem. Theory Comput.* **1**, 153–168 (2005).

[17] Bartlett, R. J. and Purvis, G. D. *Int. J. Quantum Chem.* **14**, 561 (1978).

[18] Boys, S. F. and Bernardi, F. Calculation of small molecular interactions by differences of separate total energies - some procedures with reduced errors. *Mol. Phys.* **19**, 553 (1970).

[19] Ryckaert, J. P., Ciccotti, G., and Berendsen, H. J. C. Numerical integration of the cartesian equations of motion of a system with constraints; molecular dynamics of n-alkanes. *J. Comp. Phys.* **23**, 327–341 (1977).

[20] Miyamoto, S. and Kollman, P. A. SETTLE: An analytical version of the SHAKE and RATTLE algorithms for rigid water models. *J. Comput. Chem.* **13**, 952–962 (1992).

[21] van der Spoel, D., van Maaren, P. J., and Caleman, C. GROMACS molecule & liquid database. *Bioinformatics* **28**, 752–753 (2012).

[22] Lamoureux, G. and Roux, B. Absolute hydration free energy scale for alkali and halide ions established from simulations with a polarizable force field. *J. Phys. Chem. B.* **110**, 3308–3322 (2006).

[23] Bussi, G., Donadio, D., and Parrinello, M. Canonical sampling through velocity rescaling. *J Chem Phys* **126**(1), 014101 Jan (2007).

[24] Berendsen, H. J. C., Postma, J. P. M., DiNola, A., and Haak, J. R. Molecular dynamics with coupling to an external bath. *J. Chem. Phys.* **81**, 3684–3690 (1984).

[25] Darden, T., York, D., and Pedersen, L. Particle mesh Ewald: An N-log(N) method for Ewald sums in large systems. *J. Chem. Phys.* **98**, 10089–10092 (1993).

[26] Caleman, C., Hub, J. S., van Maaren, P. J., and van der Spoel, D. Atomistic simulation of ion solvation in water explains surface preference of halides. *Proc. Natl. Acad. Sci. U.S.A.* **108**, 6838–6842 (2011).

[27] Lamoureux, G., MacKerell, A. D., and Roux, B. A simple polarizable model of water based on classical drude oscillators. *J. Chem. Phys.* **119**, 5185–5197 (2003).

[28] van Gunsteren, W. F. and Berendsen, H. J. C. A leap-frog algorithm for stochastic dynamics. *Mol. Sim.* **1**, 173–185 (1988).

[29] Hess, B. Determining the shear viscosity of model liquids from molecular simulation. *J. Chem. Phys.* **116**, 209–217 (2002).

[30] van der Spoel, D., Lindahl, E., Hess, B., Groenhof, G., Mark, A. E., and Berendsen, H. J. C. GROMACS: Fast, Flexible and Free. *J. Comput. Chem.* **26**, 1701–1718 (2005).

[31] Hess, B., Kutzner, C., van der Spoel, D., and Lindahl, E. GROMACS 4: Algorithms for highly efficient, load-balanced, and scalable molecular simulation. *J. Chem. Theory Comput.* **4**, 435–447 (2008).

[32] Yu, H., Whitfield, T. W., Harder, E., Lamoureux, G., Vorobyov, I., Anisimov, V. M., MacKerell, Jr., A. D., and Roux, B. Simulating monovalent and divalent ions in aqueous solution using a drude polarizable force field. *J. Chem. Theory Comput.* **6**, 774–786 (2010).

[33] Wennberg, C. L., Murtola, T., Hess, B., and Lindahl, E. Lennard-jones lattice summation in bilayer simulations has critical effects on surface tension and lipid properties. *J. Chem. Theory Comput.* **9**, 3527–3537 (2013).

[34] Sun, L., Li, X., Hede, T., Tu, Y., Leck, C., and Agren, H. Molecular dynamics simulations of the surface tension and structure of salt solutions and clusters. *J. Phys. Chem. B.* **116**, 3198–3204 (2012).

[35] Zubillaga, R. A., Labastida, A., Cruz, B., Martinez, J. C., Sanchez, E., and Alejandre, J. Surface tension of organic liquids using the opls/aa force field. *J. Chem. Theory Comput.* **9**, 1611–1615 (2013).

[36] Park, M., Shin, I., Singh, N., and Kim, K. Eigen and zundel forms of small protonated water clusters: structures and infrared spectra. *J. Phys. Chem. A* **111**, 10692–10702 (2007).

[37] Tuckerman, M., Laasonen, K., Sprik, M., and Parrinello, M. Ab initio molecular dynamics simulation of the solvation and transport of hydronium and hydroxyl ions in water. *J. Chem. Phys.* **103**, 150 (1995).

[38] Bucher, D., Gray-Weale, A., and Kuyucak, S. Ab initio study of water polarization in the hydration shell of aqueous hydroxide: comparison between polarizable and nonpolarizable water model. *J. Chem. Theory Comp.* **6**, 2888–2895 (2010).

[39] Tuckerman, M., Chandra, A., and Marx, D. Structure and dynamics of OH- (aq). *Acc. Chem. Res.* **39**, 151–158 (2006).

[40] Tuckerman, M., Marx, D., and Parrinello, M. The nature and transport mechanism of hydrated hydroxide ions in aqueous solution. *Nature* **417**, 925–929 (2002).

[41] Knight, C., Maupin, C., Izvekov, S., and Voth, G. Defining condensed phase reactive force fiels from ab initio dynamics simulations: the case of the hydrated excess proton. *J. Chem. Theory Comput.* **6**, 3223–3232 (2010).

[42] Asthagiri, D., Pratt, L., and Kress, J. Ab initio molecular dynamics ans quasichemical study of h+(aq). *Proc. Natl. Acad. Sci. U.S.A.* **102**, 6704–6708 (2005).

[43] Markovitcha, O. and Agmon, N. Reversible geminate recombination of hydrogen-bonded water molecule pair. *J. Chem. Phys.* **129**, 084505 (2008).

[44] Swanson, J. and Simons, J. Role of charge transfer in strucutre and dynamics of the hydrated proton. *J. Phys. Chem. B.* **113**, 5149–5161 (2009).

[45] Heuft, J. and Meijer, H. A density functional theory based study of the microscopic structure and dynamics of aqueous hcl solutions. *Phys. Chem. Chem. Phys.* **8**, 3116–3123 (2006).

[46] Zie, Z., Bau, R., and Reed, C. A crystalline [h9o4]+ hydronium ion salt with a weakly coordinating anion. *Inorg. Chem.* **34**, 5403–5404 (1995).

[47] Stoyanov, E., Stoyanova, I., Tham, F., and Reed, C. H_{aq}^+ structure in proton wires inside nanotubes. *J. Am. Chem. Soc.* **131**, 17540–17541 (2009).

[48] Botti, A., Bruni, F., Imberti, S., Ricci, M., and Soper, A. Ion in water: The microscopic structure of a concentrated HCl solution. *J. Chem Phys.* **121**, 7840–7848 (2004).

[49] Marx, D., Tuckerman, M., Hutter, J., and Parrinello, M. The nature of the hydrated excess proton inwater. *Nature* **397**, 601–604 (1999).

[50] Fulton, J. and Balasubramanian, M. Structure of hydronium (h3o+)/chloride(cl-) contact ion pairs in aqueous hydrochloric acid solution: A zundel-like local configuration. *J. Am. Chem. Soc.* **132**, 12597–12604 (2010).

[51] Xu, J., Zhang, Y., and Voth, G. Infrared spectrum of the hydrated proton in water. *Phys. Chem. Lett.* **2**, 81–86 (2011).

[52] Ufimtsev, I., Kalinichev, A., Martinez, T., and Kirkpatrick, R. A chraged ring model for classical OH- (aq) simulations. *Chem. Phys. Lett.* **442**, 128–133 (2007).

[53] McLain, S., Imberti, S., Soper, A., Botti, A., Bruni, F., and Ricci, M. Structure of 2 molar naoh in aqueous solution from neutron diffraction and empirical potential structural refinement. *Phys. Rev. B* **74**, 094201 (2006).

[54] Megyes, T., Bálint, S., Grósz, T., Radnai, T., Bakó, I., and Sipos, P. The structure of aqueous sodium hydroxide solutions: A combined solution x-ray diffraction and simulation study. *J. Chem. Phys.* **128**(4), 044501–12 (2008).

[55] Śmiechowski, M. and Stangret, J. Hydroxide ion hydration in aqueous solutions. *J. Phys. Chem. A* **111**, 2889–2897 (2007).

[56] Botti, A., Bruni, F., Imberti, S., Ricci, M., and Soper, A. Solvation of hydroxyl ions in water. *J. Chem. Phys.* **119**, 5001–5004 (2003).

[57] Buch, V., Milet, A., Vácha, R., Jungwirth, P., and Devlin, J. P. Water surface is acidic. *Proc. Natl. Acad. Sci. U.S.A.* **104**, 7342–6347 (2007).

[58] Henry, C. L., Dalton, C. N., Scruton, L., and Craig, V. S. J. Ion-specific coalescence of bubbles in mixed electrolyte solutions. *J. Phys. Chem. C.* **111**, 1015–1023 (2007).